Complex Contact-Based Dynamics of Microsphere Monolayers Revealed by Resonant Attenuation of Surface Acoustic Waves

M. Hiraiwa,[1] M. Abi Ghanem,[1] S. P. Wallen,[1] A. Khanolkar,[1] A. A. Maznev,[2] and N. Boechler[1]
[1]Department of Mechanical Engineering, University of Washington, Seattle, Washington 98195, USA
[2]Department of Chemistry, Massachusetts Institute of Technology, Cambridge, Massachusetts 02139, USA
(Received 7 December 2015; published 11 May 2016)

Contact-based vibrations play an essential role in the dynamics of granular materials. Significant insights into vibrational granular dynamics have previously been obtained with reduced-dimensional systems containing macroscale particles. We study contact-based vibrations of a two-dimensional monolayer of micron-sized spheres on a solid substrate that forms a microscale granular crystal. Measurements of the resonant attenuation of laser-generated surface acoustic waves reveal three collective vibrational modes that involve displacements and rotations of the microspheres, as well as interparticle and particle-substrate interactions. To identify the modes, we tune the interparticle stiffness, which shifts the frequency of the horizontal-rotational resonances while leaving the vertical resonance unaffected. From the measured contact resonance frequencies we determine both particle-substrate and interparticle contact stiffnesses and find that the former is an order of magnitude larger than the latter. This study paves the way for investigating complex contact-based dynamics of microscale granular crystals and yields a new approach to studying micro- to nanoscale contact mechanics in multiparticle networks.

DOI: 10.1103/PhysRevLett.116.198001

Micro- and nanoscale particles in contact with other bodies experience strong adhesive forces that induce deformation near the point of contact [1]. The understanding of contact mechanics is critical to many fields, including areas such as surface science [1], contaminant removal [2], self-assembly [3], powder technology and processing [4,5], and biomedicine [6]. In systems with adhered micro- and nanoscale particles, low frequency dynamic disturbances (compared to the intrinsic spheroidal modes of the spheres [7]) can induce contact-based vibrational modes in single- and multiparticle systems, where the particles move like rigid bodies and the local region of deformation around the contact acts as a spring [8].

Such contact-based vibrational modes form the foundation for the dynamics of particulate assemblies. The contact-based dynamics of granular media play a critical role in fields such as wave propagation in geological and other microstructured materials [8]. While there has been significant progress in the study of the contact-based dynamics of macroscale granular media [8,9], the dynamics of micro- to nanoscale particle assemblies are less understood. This difference in scale is important from a fundamental perspective; in particular, adhesion forces negligible for macroscale particles become critical at micro- to nanoscales.

At the macroscale, studies of reduced dimensional systems, such as one- and two-dimensional granular arrays that are commonly referred to as "granular crystals," have yielded significant insights into the dynamics of granular materials [8,9]. In contrast, studies of the contact-based dynamics of micro- to nanoscale particle assemblies have hitherto been restricted to three-dimensional, typically disordered, settings [8,10–12]. Recently, a contact resonance of microspheres assembled into a two-dimensional monolayer adhered to a solid substrate was measured via its hybridization with surface acoustic waves (SAWs) traveling in the substrate [13]. The results agreed well with a simple model where the particle motion was restricted to the vertical (out-of-plane) degree of freedom and the interaction between the particles was disregarded. However, models involving both rotations and interparticle interactions [14,15] predicted more complex dynamics. For motion in the sagittal plane, a close-packed monolayer of spheres on a solid substrate is expected to yield three collective contact-based vibrational modes: one predominantly vertical, and two of mixed horizontal-rotational character, all of which should interact with SAWs [14]. It has remained a mystery as to why the previous experiment only showed the presence of a single contact resonance mode.

In this work, we reveal the presence of all three contact resonances predicted for the microsphere monolayer, by measuring the attenuation of SAWs using a scanned laser ultrasonic technique. We test the model by changing the interparticle contact stiffness via the deposition of a thin aluminum film on top of the spheres, which shifts the horizontal-rotational contact resonance frequencies upwards. We further confirm the nature of the modes using a complementary laser-ultrasonic technique that preferentially excites the vertical contact resonance. In addition to providing direct evidence of the rotational-vibrational dynamics of microgranular media, our work opens a new approach for the study of micro- to nanoscale particle contact mechanics by enabling measurements of both the

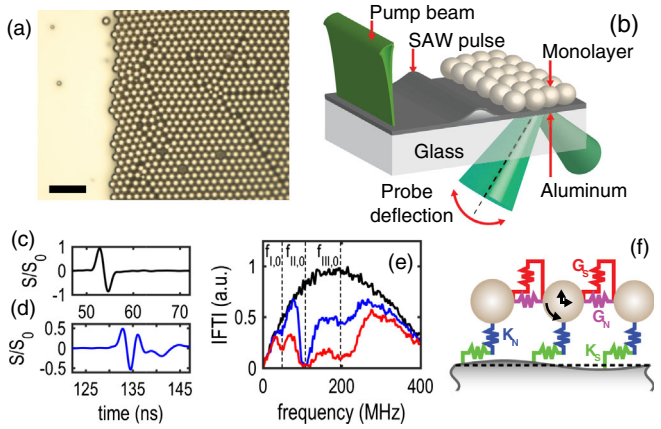

FIG. 1. Overview of the experiment. (a) Microscope image of the interface between the monolayer and blank sample regions. The scale bar is 10 μm. (b) Schematic of the laser ultrasonic experimental setup. Normalized signal measured in the (c) blank region and (d) 132 μm inside the monolayer region. (e) Normalized Fourier spectra of the signals in (c) and (d) using the same colors. The red spectrum corresponds to a signal measured 400 μm inside the monolayer region. The vertical dashed lines denote the identified contact resonance frequencies. (f) Schematic of the dynamical model.

interparticle and particle-substrate contact stiffness and offering insight into the role of shear contact rigidity.

Our sample is a monolayer of $D = 2.0$ μm diameter silica microspheres deposited on an aluminum-coated glass substrate, as shown in Figs. 1(a) and 1(b). The aluminum layer is 100 nm thick, and the glass is 1.5 mm thick. A wedge-shaped cell convective self-assembly technique is used to assemble the monolayer on the substrate [16]. To obtain a planar interface between substrate regions with and without the microsphere monolayer (hereafter referred to as the monolayer and blank regions, respectively), we use a microcontact-printing method, wherein a soft polydimethylsiloxane stamp is pressed into conformal contact with the microsphere monolayer and then is removed, such that the spheres detach from the substrate in the stamped region [17,18]. A representative optical microscope image of the resulting interface is shown in Fig. 1(a).

To generate and measure SAW propagation in our sample, we utilize a scanning laser-ultrasonic technique, as shown in Fig. 1(b) [18]. We focus a subnanosecond laser pulse, which serves as a "pump," into a line on the aluminum surface of the blank region of the substrate. The absorbed laser light launches broadband SAW pulses that propagate as plane waves perpendicular to the line source. The acoustic response of the sample is measured via a knife-edge photodeflection technique [22]. A "probe" beam is incident through the substrate and focused to a small spot on the aluminum film. The reflected probe light is focused onto a fast photodetector, after being partially blocked by a knife edge. Changes in the surface slope and refractive index caused by the SAWs deflect the probe beam, which translates to a change in intensity on the photodetector. To obtain spatial information, the sample is automatically scanned in the direction of the SAW propagation. Both the pump and probe are initially focused onto the blank region, then moved progressively closer to the interface, with the probe crossing into the monolayer region.

Figures 1(c) and 1(d) show typical measured signals S, normalized to the maximum signal amplitude S_0 measured during the scan. Figure 1(c) corresponds to a probe position in the blank region, and Fig. 1(d) corresponds to a probe position 132 μm inside the monolayer region. The distortion of the signal in Fig. 1(d) is a result of dispersion and dissipation induced by the monolayer.

The Fourier spectra of the normalized signals in Figs. 1(c) and 1(d) are shown in Fig. 1(e). The spectrum corresponding to the signal in the monolayer region shows a sharp dip at 108 MHz. We also observe two smaller dips surrounding this resonance, and denote the three dips with vertical lines drawn at $f_{\mathrm{I},0} = 49$ MHz, $f_{\mathrm{II},0} = 108$ MHz, $f_{\mathrm{III},0} = 197$ MHz. We also show a third spectrum, corresponding to a location 400 μm inside the monolayer region, which demonstrates the evolution of the attenuation zones.

To obtain position-dependent transmission spectra of SAWs traversing the interface, we normalize the Fourier spectra at each position by the average Fourier spectra of the incident SAW (averaged over all positions in the blank region). Figure 2(a) shows the measured transmission spectra as a function of distance from the interface. Three distinct attenuation maxima are evident, corresponding to the identified dips in Fig. 1(e). We interpret the measured attenuation maxima as being caused by the interaction of SAWs with contact resonances of the microsphere monolayer, as described by the recently developed model of Ref. [14]. In this model, the microspheres are considered as rigid bodies, and the sphere-substrate and sphere-sphere contacts are represented as normal and shear springs, as is shown in Fig. 1(f). This model predicts three collective vibrational modes of the monolayer involving vertical, horizontal, and rotational motion of spheres in the sagittal plane.

At long wavelengths (compared to the particle spacing), one of the modes is purely vertical, with a frequency given by

$$f_N = \frac{1}{2\pi}\left[\frac{K_N}{m}\right]^{1/2}, \tag{1}$$

while two others are of mixed horizontal-rotational character, with frequencies given by

$$f_{\mathrm{RH}} = \frac{1}{2\pi}\left[\left(\frac{K_S}{4m}\right)\left(20\gamma + 7 + \sqrt{400\gamma^2 + 120\gamma + 49}\right)\right]^{1/2},$$
$$f_{\mathrm{HR}} = \frac{1}{2\pi}\left[\left(\frac{K_S}{4m}\right)\left(20\gamma + 7 - \sqrt{400\gamma^2 + 120\gamma + 49}\right)\right]^{1/2}, \tag{2}$$

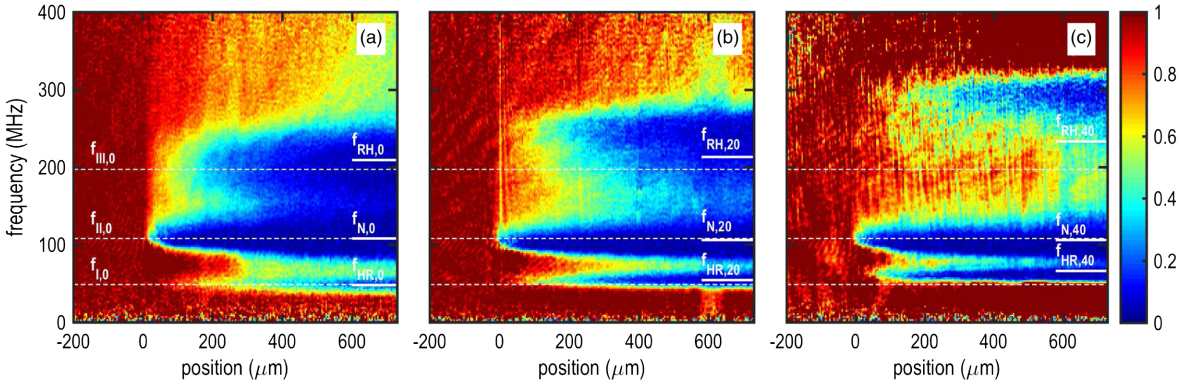

FIG. 2. (a)–(c) Transmission spectra for SAWs propagating across the interface between the blank and monolayer regions. The color bar denotes the magnitude of the transmission coefficient. The horizontal dashed lines denote the identified contact resonance frequencies for the uncoated monolayer. The short horizontal lines on the right of the panels are the fitted contact resonance frequencies. Position denotes the distance from the interface. (a) Uncoated microsphere monolayer. (b) 20 nm of aluminum coating. (c) 40 nm of aluminum coating.

where $m = \rho\pi D^3/6$ is the microsphere mass, K_N is the particle-substrate normal stiffness, K_S is the particle-substrate shear stiffness, G_S is the interparticle shear stiffness, and $\gamma = G_S/K_S$. The interparticle normal contact stiffness G_N does not affect these resonances at long wavelengths. The frequency f_{RH} corresponds to the predominantly rotational mode and is always higher than the frequency of the predominantly horizontal mode f_{HR}. If the monolayer is placed on an elastic substrate, all three modes are predicted to interact with SAWs [14]. In the absence of dissipation, this interaction results in the hybridization and avoided crossing of the Rayleigh SAW with the contact resonances. In the presence of dissipation, avoided crossing may or may not take place, but one would invariably expect a peak in attenuation at the contact resonance frequency [23]. As can be seen from Eqs. (1) and (2), f_N is determined solely by the particle-substrate contact, whereas f_{RH} and f_{HR} are affected by both contacts. Hence, if we increase the interparticle contact stiffness, only f_{RH} and f_{HR} are expected to increase.

To test the model and verify the nature of the observed contact resonances, we coat the microsphere monolayer with a thin aluminum layer using electron beam evaporation, which stiffens the interparticle contact without affecting the particle-substrate contact [18]. Figures 2(b) and 2(c) show transmission spectra for the samples coated with aluminum. The highest and the lowest attenuation maxima shift upwards upon the deposition of the aluminum, while the middle maximum remains nearly unaffected. The relatively small downshift of the middle resonance, which is approximately consistent with the predicted frequency downshift of ~4% due to extra mass loading, confirms our assignment of the middle resonance to f_N. In all cases, the middle zone has the largest attenuation, indicating stronger coupling of this resonance to the propagating SAWs.

For further confirmation of the assignment of the resonances, we conduct a separate experiment on the sample coated with 40 nm of aluminum, wherein a pump beam entering through the substrate is focused to a large diameter (240 μm at $1/e^2$ intensity level) spot. In this configuration, thermal expansion of the aluminum layer excites the vertical contact resonance of the spheres directly, while horizontal-rotational resonances are not excited because of symmetry constraints. The displacement of the spheres is measured with a grating interferometer [24], which is also only sensitive to vertical motion. The measured signal shown in Fig. 3(b) contains oscillations at a frequency of ~100 MHz, as can be seen from the Fourier spectrum in Fig. 3(c), thus confirming the middle resonance in Figs. 2(a)–2(c) as the vertical mode.

We compare the frequencies of the observed attenuation maxima shown in Fig. 2 with those predicted by Eqs. (1) and (2). While the equations have three unknown parameters (K_N, K_S, and G_S), we relate K_S to K_N via the Hertz-Mindlin contact model [25], which leaves two independent parameters. In the Hertz-Mindlin contact model, assuming a no-slip condition at the contact, the normal stiffness for a given contact is related to the shear stiffness, such that $K_S/K_N = 4G^*/E^*$, where $E^* = [(1-\nu_1^2)/E_1 + (1-\nu_2^2)/E_2]^{-1}$ is the effective Young's modulus of the contact and $G^* = [(2-\nu_1)/G_1 + (2-\nu_2)/G_2]^{-1}$ is the effective shear modulus, where E_1 and G_1 are the moduli for the silica

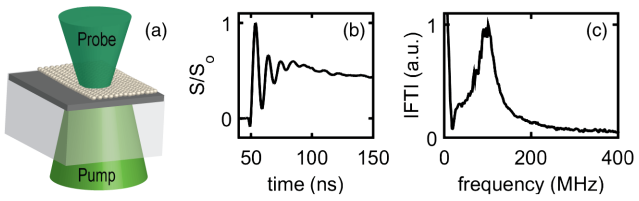

FIG. 3. (a) Schematic of the experiment with large spot excitation and grating interferometer detection. (b) Normalized signal measured with the interferometer. (c) Fourier spectrum of the signal in (b).

microspheres, and E_2 and G_2 are the moduli for the aluminum substrate [18]. Using Eq. (1) and the measured value of $f_{\mathrm{II},0} = f_N$, we find a particle-substrate normal contact stiffness of $K_N = 4.0$ kN/m, and thus also obtain the particle-substrate shear stiffness $K_S = 3.5$ kN/m. We then use a least-squares fit to determine the interparticle shear stiffness G_S, where the quantity $[(f_{\mathrm{I}} - f_{\mathrm{HR}})/f_{\mathrm{I}}]^2 + [(f_{\mathrm{III}} - f_{\mathrm{RH}})/f_{\mathrm{III}}]^2$ is minimized, with f_{HR} and f_{RH} defined as in Eq. (2). For the uncoated sample, we obtain an interparticle shear stiffness of $G_S = 0.3$ kN/m [18]. In Fig. 2, we denote the fitted contact resonance frequencies using white solid lines on the right side of each panel. For the uncoated sample, we see an excellent agreement between the measured attenuation frequencies and the fitted contact resonance frequencies. For the sample coated with 40 nm of aluminum, the agreement is not as good. This difference may be due to deviations from the physical scenario described by our model due to the presence of the aluminum, including asymmetric interparticle contacts and the formation of "necks," which may lead to bending resistance not taken into account in the model.

A particularly intriguing result is that the interparticle shear contact stiffness is over an order of magnitude smaller than the particle-substrate contact stiffnesses. As a comparison, we use the Hertz-Mindlin elastic contact model with the DMT model of an adhesive contact [26] to calculate theoretical contact stiffnesses. This results in predicted stiffnesses $K_{N,\mathrm{DMT}} = 1.6$ kN/m, $K_{S,\mathrm{DMT}} = 1.4$ kN/m, and $G_{S,\mathrm{DMT}} = 0.8$ kN/m, which gives a ratio of less than 2 between the particle-substrate and interparticle stiffnesses. Consistent with the trend observed in recent studies [13,27], the measured particle-substrate normal contact stiffness is also over twice as large as predicted. A discrepancy between the estimated and measured values can be ascribed to factors such as uncertainty in the work of adhesion [1], plastic deformation, which may stiffen the contact [28,29], or microslip at the contact, which may decrease the shear contact stiffness [30]. For instance, prior studies have shown higher than predicted adhesion between dielectrics and reactive metals such as aluminum [31]. In addition, an examination of SEM images [18] showed that the interparticle contact network is not uniform: even in closely packed regions, most particles do not form adhesive contacts with all six neighbors. This raises the question of how adhesive contact networks form following self-assembly, and may contribute to lower than predicted interparticle contact stiffnesses. Our measurement approach offers a unique opportunity to investigate this issue.

We have also studied the effect of the microspheres on SAW dispersion. Figure 4 shows the normalized magnitude of the two-dimensional Fourier transform of the scanned measurements taken in the monolayer region. Figure 4(a) shows spectra corresponding to the uncoated sample. Figure 4(b) shows spectra corresponding to the sample with 40 nm of aluminum. The spectra show a line

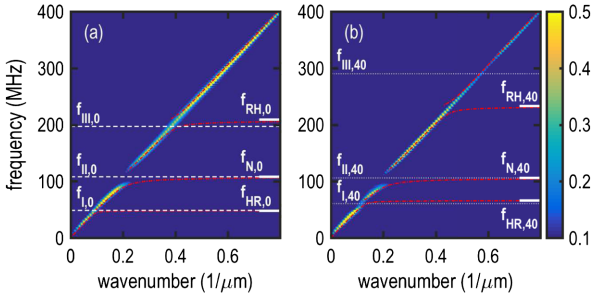

FIG. 4. Surface acoustic wave dispersion in samples with (a) an uncoated monolayer and (b) a 40 nm thick aluminum coating. The color plot denotes the normalized magnitude of the calculated 2D Fourier spectra. The horizontal dashed and dotted lines correspond to the identified contact resonance frequencies for the uncoated sample and the sample with 40 nm of aluminum, respectively. The short horizontal lines on the right of the panels are the fitted contact resonance frequencies. The red dash-dotted lines are the dispersion curves calculated using the fitted resonance frequencies.

corresponding to Rayleigh SAWs in the substrate, which has three gaps or regions of attenuation corresponding to the attenuation zones seen in Fig. 2. The highest and lowest zones appear as lighter-colored, attenuated regions, whereas the middle zone shows a clear gap with a curvature indicative of an avoided crossing. An emerging band gap can also be seen at the lowest resonance in Fig. 4(b).

Using the fitted contact resonance frequencies with the effective medium model for a monolayer of microspheres on an elastic substrate [14], we plot the calculated dispersion curves as the red dash-dotted lines in Fig. 4 [18]. For the strong middle resonance and also the emerging avoided crossing at the lowest resonance in Fig. 4(b), we see reasonable agreement between experiment and theory in the curvature of the branches, which confirms that our model captures the coupling strength between the contact resonances and the SAWs. For resonances with weak coupling and low quality factors, hybridization gaps can appear as attenuation zones instead of avoided crossings [23], which explains why weaker horizontal-rotational resonances were not identified previously in Ref. [13].

This work opens the door for the study of the contact-based dynamics of low-dimensional microgranular systems, which, in contrast to their macroscale counterparts [9], may have additional acousto-optic [32] or acousto-plasmonic [33] functionalities, be rapidly and inexpensively manufactured via self-assembly, and find future use in chip-scale applications. The discovery of collective vibrational modes including rotations as well as displacements, along with the characterization of shear and normal contact stiffnesses in microscale particle assemblies, will lead to better and broader understanding of wave propagation in microgranular media with applications in shock mitigation, energetic materials, seismic exploration, and powder processing, and have implications for future studies of colloidal crystal

systems [34,35]. This study reveals the critical role of particle rotations: for instance, without rotations, the upper rotational-horizontal resonance would not be present [14]. Our characterization method is complementary to existing techniques [36–39], as it is noncontact and nondestructive, offers information about equilibrium contact stiffnesses, and, in contrast to other dynamic techniques involving isolated particles [36–38], enables the measurement of the interparticle contact stiffness in a microscale multiparticle assembly. Finally, the sensitivity to contact forces in the microgranular monolayer may be used in sensors for bioanalytical [40] and other applications.

This work was supported by the U.S. National Science Foundation (Grant No. CMMI-1333858), the U.S. Army Research Office (Grant No. W911NF-15-1-0030), and the University of Washington Royalty Research Foundation. The contribution by A. A. M. was supported by National Science Foundation Grant No. CHE-1111557. M. H. acknowledges support from the National Science Foundation Graduate Research Fellowship Program under Grant No. DGE-1256082.

[1] J. N. Israelachvili, *Intermolecular and Surface Forces*, 3rd. ed. (Academic Press, Waltham, MA, 2011).
[2] K. L. Mittal and R. Jaiswal, *Particle Adhesion and Removal* (Wiley-Scrivener, Beverly, MA, 2015).
[3] Y. Min, M. Akbulut, K. Kristiansen, Y. Golan, and J. Israelachvili, The role of interparticle and external forces in nanoparticle assembly, Nat. Mater. **7**, 527 (2008).
[4] J. Duran, *Sands, Powders, and Grains: An Introduction to the Physics of Granular Materials* (Springer, New York, 2000).
[5] H. Masuda, K. Higashitani, and H. Yoshida, *Powder Technology Handbook*, 3rd ed. (CRC Press, Boca Raton, FL, 2006).
[6] P. A. L. Fernandes, M. Delcea, A. G. Skirtach, H. Möhwald, and A. Fery, Quantification of release from microcapsules upon mechanical deformation with AFM, Soft Matter **6**, 1879 (2010).
[7] Y. Sato and T. Usami, Basic Study on the oscillation of a homogeneous elastic sphere, Geophysical Magazine **31**, 15 (1962).
[8] V. Nesterenko, *Dynamics of Heterogeneous Materials* (Springer, New York, NY, 2001).
[9] G. Theocharis, N. Boechler, and C. Daraio, *Nonlinear Periodic Phononic Structures and Granular Crystals, Acoustic Metamaterials and Phononic Crystals* (Springer, Heidelberg, 2013), pp. 217–251.
[10] M. Mattarelli, M. Montagna, T. Still, D. Schneider, and G. Fytas, Vibration spectroscopy of weakly interacting mesoscopic colloids, Soft Matter **8**, 4235 (2012).
[11] D. Schneider, M. Schmitt, C. M. Hui, R. Sainidou, P. Rembert, K. Matyjaszewski, M. R. Bockstaller, and G. Fytas, Role of polymer graft architecture on the acoustic eigenmode formation in densely polymer-tethered colloidal particles, ACS Macro Lett. **3**, 1059 (2014).
[12] A. Ayouch, X. Dieudonné, G. Vaudel, H. Piombini, K. Vallé, V. Gusev, P. Belleville, and P. Ruello, Elasticity of an assembly of disordered nanoparticles interacting via either Van der Waals-bonded or covalent-bonded coating layers, ACS Nano **6**, 10614 (2012).
[13] N. Boechler, J. K. Eliason, A. Kumar, A. A. Maznev, K. A. Nelson, and N. Fang, Interaction of a contact resonance of microspheres with surface acoustic waves, Phys. Rev. Lett. **111**, 036103 (2013).
[14] S. P. Wallen, A. A. Maznev, and N. Boechler, Dynamics of a monolayer of microspheres on an elastic substrate, Phys. Rev. B **92**, 174303 (2015).
[15] V. Tournat, I. Pèrez-Arjona, A. Merkel, V. Sanchez-Morcillo, and V. Gusev, Elastic waves in phononic monolayer granular membranes, New J. Phys. **13**, 073042 (2011).
[16] J. Sun, C. J. Tang, P. Zhan, Z. I. Han, Z. S. Cao, and Z. L. Wang, Fabrication of centimeter-sized single-domain two-dimensional colloidal crystals in a wedge-shaped cell under capillary forces, Langmuir **26**, 7859 (2010).
[17] B. H. Lee, H. Shin, and M. M. Sung, Patterning a two-dimensional colloidal crystal by water-mediated particle transfer printing, Chem. Mater. **19**, 5553 (2007).
[18] See Supplemental Material at http://link.aps.org/supplemental/10.1103/PhysRevLett.116.198001, which includes Refs. [19–21], for additional details on the experimental setups and signal processing, SEM images of the monolayer, the identified and fitted contact resonance frequencies, and the material properties used in the calculations.
[19] N. P. Bansal and R. H. Doremus, *Handbook of Glass Properties* (Academic Press, Orlando, 1986).
[20] ASM International Handbook Committee, *Properties and Selection: Nonferrous Alloys and Special-Purpose Alloys, ASM Handbook* (ASM International, Materials Park, OH, 1990), Vol. 2.
[21] M. Haldimann, A. Luible, and M. Overend, *Structural Use of Glass* (International Associate for Bridge and Structural Engineering, Zurich, 2008).
[22] C. B. Scruby and L. E. Drain, *Laser Ultrasonics: Techniques and Applications* (Taylor & Francis, New York, 1990).
[23] E. A. Garova, A. A. Maradudin, and A. P. Mayer, Interaction of Rayleigh waves with randomly distributed oscillators on the surface, Phys. Rev. B **59**, 13291 (1999).
[24] C. Glorieux, J. D. Beers, E. H. Bentefour, K. Van de Rostyne, and K. A. Nelson, Phase mask based interferometer: Operation principle, performance, and application to thermoelastic phenomena, Rev. Sci. Instrum. **75**, 2906 (2004).
[25] R. D. Mindlin, Compliance of elastic bodies in contact, J. Appl. Mech. **16**, 259 (1949).
[26] V. M. Muller, B. V. Derjaguin, and Yu. P. Toporov, On two methods of calculation of the force of sticking of an elastic sphere to a rigid plane, Colloids Surf. **7**, 251 (1983).
[27] A. Khanolkar, S. P. Wallen, M. Abi Ghanem, J. Jenks, N. Vogel, and N. Boechler, A self-assembled metamaterial for Lamb waves, Appl. Phys. Lett. **107**, 071903 (2015).
[28] X. D. Wang, Z. X. Shen, J. L. Zhang, H. F. Jiao, X. B. Cheng, X. W. Ye, KL. Y. Chen, and Z. H. Wang, Contact between submicrometer silica spheres, Langmuir **26**, 5583 (2010).

[29] J. N. D'Amour, J. J. R. Stalgren, K. K. Kanazawa, C. W. Frank, M. Rodahl, and D. Johannsmann, Capillary aging of the contacts between glass spheres and a quartz resonator surface, Phys. Rev. Lett. **96**, 058301 (2006).

[30] K. L. Johnson, *Contact Mechanics* (Cambridge University Press, Cambridge, 1985).

[31] D. M. Lipkin, J. N. Israelachvili, and D. R. Clarke, Estimating the metal-ceramic van der Waals adhesion energy, Philos. Mag. A **76**, 715 (1997).

[32] A. V. Akimov, Y. Tanaka, A. B. Pevtsov, S. F. Kaplan, V. G. Golubev, S. Tamura, D. R. Yakovlev, and M. Bayer, Hypersonic modulation of light in three-dimensional photonic and phononic band-gap materials, Phys. Rev. Lett. **101**, 033902 (2008).

[33] P. M. Jais, D. B. Murray, R. Merlin, and A. V. Bragas, Metal nanoparticle ensembles: Tunable laser pulses distinguish monomer from dimer vibrations, Nano Lett. **11**, 3685 (2011).

[34] P. J. Yunker, K. Chen, M. D. Gratale, M. A. Lohr, T. Still, and A. G. Yodh, Physics in ordered and disordered colloidal matter composed of poly(N-isopropyl acrylamide) microgel particles, Rep. Prog. Phys. **77**, 056601 (2014).

[35] B. Li, F. Wang, D. Zhou, Y. Peng, R. Ni, and Y. Han, Modes of surface premelting in colloidal crystals composed of attractive particles, Nature (London) **531**, 485 (2016).

[36] M. D. Murthy Peri and C. Cetinkaya, Non-contact microsphere–surface adhesion measurement via acoustic base excitations, J. Colloid Interface Sci. **288**, 432 (2005).

[37] E. Vittorias, M. Kappl, H. J. Butt, and D. Johannsmann, Studying mechanical microcontacts of fine particles with the quartz crystal microbalance, Powder Technol. **203**, 489 (2010).

[38] Y. Guillet, B. Audoin, M. Ferrié, and S. Ravaine, All-optical ultrafast spectroscopy of a single nanoparticle-substrate contact, Phys. Rev. B **86**, 035456 (2012).

[39] R. Fuchs, T. Weihart, J. Meyer, H. Zhuang, T. Staedler, X. Jiang, and S. Luding, Rolling, sliding and torsion of micron-sized silica particles: experimental, numerical and theoretical analysis, Granular Matter **16**, 281 (2014).

[40] T. M. A. Gronewold, Surface acoustic wave sensors in the bioanalytical field: Recent trends and challenges, Anal. Chim. Acta **603**, 119 (2007).